International Journal of Low-Carbon Technologies, 2026, **21**, 1–14, ctag026
https://doi.org/10.1093/ijlct/ctag026
Original Article

OXFORD

CFD-based analysis of chimney performance optimization for the Manzanares pilot plant

Pinar Mert Cuce[1,2], Erdem Cuce[3,4,5,*], Saad Alshahrani[6,7]

[1]Department of Architecture, Faculty of Engineering and Architecture, Recep Tayyip Erdogan University, Zihni Derin Campus, 53100 Rize, Turkey
[2]Department of Architecture and Built Environment, School of Architecture, Built Environment, Computing and Engineering, Birmingham City University, Birmingham B4 7XG, United Kingdom
[3]Department of Mechanical Engineering, Faculty of Engineering and Architecture, Recep Tayyip Erdogan University, Zihni Derin Campus, 53100 Rize, Turkey
[4]University Centre for Research and Development, Chandigarh University, Mohali, Punjab 140413, India
[5]Center for Research Impact and Outcome, Chitkara University, Rajpura, Punjab 140401, India
[6]Department of Mechanical Engineering, College of Engineering, King Khalid University, PO Box 394, Abha 61421, Saudi Arabia
[7]Centre for Engineering and Technology Innovations, King Khalid University, Abha 61421, Saudi Arabia
*Corresponding author. Department of Mechanical Engineering, Faculty of Engineering and Architecture, Recep Tayyip Erdogan University, Zihni Derin Campus, 53100 Rize, Turkey. E-mail: erdem.cuce@erdogan.edu.tr

Abstract

This research conducts an extensive computational fluid dynamics (CFD) analysis aimed at optimizing the geometric configuration of solar chimney power plants (SCPPs), with particular emphasis on the Manzanares pilot plant. The research analyses the effects of chimney diameter and divergent chimney design on system performance under steady-state conditions at 1000 W/m^2 solar irradiance and 300 K ambient temperature. A validated three-dimensional CFD model with a 90° symmetry sector is developed in ANSYS FLUENT. The model is verified through mesh independence and benchmarked against experimental results, showing excellent agreement with measured power output and airflow velocity. The results demonstrate that chimney geometry is a dominant performance-governing factor in large-scale SCPPs. Increasing the chimney diameter up to 2.5 times the reference value enhances the power output by 97%, reaching ∼110 kW; further enlargement leads to performance deterioration due to reduced pressure potential at the turbine. More importantly, the adoption of a divergent chimney configuration yields a substantial performance improvement. An optimal chimney exit-to-inlet area ratio of 4 increases the power output to 369.4 kW, corresponding to a 5.6-fold enhancement compared to the reference cylindrical chimney. At this optimal configuration, the maximum air velocity and mass flow rate reach 28.7 m/s and 2137.8 kg/s, respectively. These findings demonstrate that multifold power enhancement can be achieved through aerodynamic optimization of chimney geometry alone, without increasing chimney height, offering a practical, cost-effective, and structurally safer design pathway for future large-scale SCPP installations.

Keywords solar chimney, chimney diameter, divergent chimney, power output

1. Introduction

Over the past decades, global energy demand has risen continuously, prompting intensified scrutiny of conventional power generation methods that have historically relied on fossil-based resources. The escalation of greenhouse gas release and environmental degradation has now reached thresholds that pose serious risks to public health, underscoring the inevitability of strict regulatory measures. Although international agreements and recently enacted protocols with defined mitigation goals have been introduced, their long-term effectiveness remains under discussion [1]. Within this context, the pursuit of substitute energy solutions capable of replacing fossil fuels has gained momentum. Such alternatives are attractive due to their low environmental footprint and their avoidance of adverse effects such as carbon emissions. These options, commonly classified as renewable energy sources, encompass a broad spectrum, including solar, wind, hydropower, and geothermal systems, all of which exhibit substantial exploitable potential [2]. Beyond electrical power production, renewable technologies are also valued for their versatility across multiple application areas. For instance, geothermal energy has been utilized for both residential and greenhouse heating, while wind power has historically supported certain agricultural processes. Among all renewables, solar energy occupies a distinctive position owing to its vast availability and applicability across diverse geographical regions. Solar resources can be harnessed directly or indirectly in nearly all locations, either in the form of thermal utilization or through specialized devices designed for electrical output. Photovoltaic technologies enable the direct conversion of incident

Received 26 February 2026. **Revised** 30 January 2026. **Accepted:** 9 February 2026

Nomenclature

A	Area (m^2)
c_p	Specific heat capacity (J/kg K)
D	Diameter (m)
D^*_{ch}	Dimensionless chimney diameter
g	Gravitational acceleration (m/s^2)
H	Height (m)
$\dot{m}$	Mass flow rate (kg/s)
P_o	Power output (kW)
P	Pressure (Pa)
Q	Volumetric flow rate (m^3/s)
R	Radius (m)
T	Temperature (K)
ΔT	Temperature difference (K)
Greek Letters	
α	Thermal diffusivity coefficient (m^2/s)
β	Thermal expansion coefficient (1/K)
η	Efficiency (%)
ν	Kinematic viscosity (m^2/s)
ρ	Density (kg/m^3)
Subscripts	
a	Ambient
coll	Collector
ch	Chimney
ch-inlet	Chimney inlet
ch-outlet	Chimney outlet
tur	Turbine

solar irradiation into electricity [3]. In addition to photovoltaic systems, other solar-based technologies exist that generate power by concentrating solar heat at a focal region and converting it into mechanical and electrical energy via thermodynamic cycles [4]. Despite their effectiveness, such systems often suffer from high capital expenditure and complex technological requirements.

An alternative solar-based electricity generation approach is the solar chimney power plant (SCPP) concept [5]. SCPPs are distinguished by their uncomplicated configuration, typically comprising a solar collector, a vertical chimney, and a turbine, and by their reliance on fundamental thermophysical mechanisms. The collector, constructed from transparent or semitransparent materials, permits solar radiation to penetrate and heat the internal air volume. The transmitted radiation reaches the ground surface, which subsequently transfers heat to the air layer beneath the collector through conduction and convection, intensified by the greenhouse effect. As the air temperature rises, density reduction occurs, inducing buoyancy-driven upward motion. Positioned centrally within the collector field, the chimney is a tall cylindrical structure that facilitates vertical airflow. Owing to the elevation difference between its base and exit, a pressure gradient is established, generating a suction effect at the chimney entrance. This pressure differential drives the heated air upward through the chimney shaft. Consequently, the airflow accelerates as it enters the chimney, converting thermal energy into kinetic energy. This kinetic energy is captured by a turbine installed at the chimney base, enabling electricity generation. Although the underlying principle of the SCPP concept is relatively old, the first operational electricity-generating installation was constructed in Spain during the 1980s and demonstrated satisfactory performance [6]. Experimental measurements from this prototype reported power outputs of ∼50 kW under solar irradiance of 1000 W/m^2 and ambient conditions of around 300 K. Following this pioneering demonstration, numerous investigations have been conducted to explore different performance aspects of SCPP systems. A significant body of literature now exists, addressing a wide range of operational parameters in detail. Reviews of laboratory-scale and pilot-scale prototypes developed for system evaluation reveal that most experimental models are substantially reduced in size compared to the original installation [2]. Experimental research has predominantly concentrated on airflow velocity fields, temperature distributions, and the influence of alternative construction materials on internal flow behaviour [7]. More recent experimental and numerical studies have further shown that absorber surface properties and ground-layer material selection play a crucial role in determining thermal storage capability, airflow dynamics, and overall system efficiency, while simultaneously introducing economic constraints related to material cost and availability [8]. Because modifying geometric configurations in physical experiments is inherently challenging, numerical modelling and computational fluid dynamics (CFD)-based analyses have become increasingly prevalent. The parameters affecting SCPP performance can generally be classified into two categories: environmental conditions and design-related factors. Environmental variables, such as solar intensity and ambient temperature, vary with location, whereas design parameters are defined by the geometric proportions and structural features of system components. A consolidated overview of studies examining these influencing factors is provided in Table 1. In addition to parametric analyses, recent review articles have integrated findings from numerical, experimental, and optimization-driven research, highlighting geometry optimization and hybrid system coupling as the most promising strategies for improving efficiency while reducing overall costs [9].

The constant pressure difference created by the chimney, acting as the main flow-inducing component of the system, necessitates careful attention, particularly in chimney sizing and design. A natural expectation is that system performance increases with incrementing chimney height. The difficulty of experimentally analysing system performance with increasing chimney height has led researchers to employ numerical and CFD studies. Ayadi *et al.* [17] construct an experimental prototype with a 2.75-m collector diameter and 3-m chimney height. A 2D CFD model validated by experimental measurements demonstrates that increasing chimney height will increase system performance. They emphasize that increasing the chimney height from 1 to 4 m boosts the maximum velocity along the chimney axis from 1.5 to 2.4 m/s. In a similar study, Kasaeian *et al.* [18] claim that the maximum airflow velocity within a chimney can be increased by 4%–25% by increasing the chimney height. These studies, which support the positive effect of increasing stack height on system performance, cannot clarify the discussion because they have not been conducted on a wide range of models and do not offer comparisons for large-scale systems. Toghraie *et al.* [19] conduct a three-dimensional CFD analysis to examine the influence of varying stack heights, from 25 to 500 m, on the performance of a SCPP featuring a 100-m collector radius and a 4-m stack radius, under solar irradiance conditions of 600 and

Table 1 Summary of published studies reporting performance parameters of SCPPs.

Reference	Performance parameters	Study details	Study findings
[10]	Solar radiation and ambient temperature	A three-dimensional CFD model was employed to examine the influence of climatic conditions on the MPP.	Results reveal that increasing solar irradiance significantly enhances power production, rising from 18 kW at 400 W/m^2 to nearly 50 kW at 1000 W/m^2. In contrast, higher ambient temperatures were found to adversely affect power output.
[11]	Chimney height	A 3D CFD analysis was conducted to investigate the impact of chimney height variation between 100 and 500 m on MPP performance.	The study shows that extending the chimney height from 200 to 500 m rises power generation from 55 kW to ∼134 kW. The results clearly highlight the chimney as the dominant component governing system performance.
[12]	Chimney diameter	A mathematical model was developed to assess the effect of varying the chimney diameter of the MPP from 10 to 30 m.	The authors report that enlarging the chimney diameter leads to a substantial performance improvement, with power output increasing from ∼52 kW at 10 m to nearly 82 kW at 30 m, corresponding to an increase of ∼60%.
[13]	Collector radius	The effect of changing the collector radius between 100 and 525 m was evaluated using a mathematical model implemented in MATLAB.	It is demonstrated that the system power output rises from around 50 kW for a reference collector radius of 122 m to ∼145 kW when the radius is incremented to 400 m under 1000 W/m^2 solar irradiation.
[14]	Collector height	A CFD-based numerical model was used to systematically analyse the influence of collector height variation from 1 to 4 m on overall system behaviour.	Findings indicate that increasing the collector height beyond the reference value of 1.85 m leads to performance degradation, with power output decreasing from ∼47 kW to nearly 33 kW at a height of 4 m.
[15]	Collector slope	The impact of collector inclination on MPP performance was examined using a CFD framework.	The results suggest that a converging collector configuration, where the inlet height is greater than the outlet height, provides improved system performance compared to alternative geometries.
[16]	Chimney angle	A three-dimensional CFD study was carried out to analyse a divergent chimney design by varying AR under 20°C ambient temperature and 1000 W/m^2 solar radiation.	The analysis shows that whilst the reference configuration produces 54.3 kW, optimal performance is achieved for AR values between 3.5 and 5, yielding a maximum power output of ∼168.5 kW.

800 W/m^2. Their results demonstrate that increasing the stack height from 100 to 500 m results in an approximately four-fold rise in power output. Notably, the study also reveals that the increase in power output does not continue indefinitely with stack height, but rather approaches a convergence point. Li *et al.* [13] develop a theoretical model grounded in the experimental data of the Manzanares pilot plant (MPP) and employ a MATLAB-based computational framework to assess the influence of varying stack heights on system performance. Their results indicate that power output increases with stack height up to ∼2000 m; however, the rate of increment significantly diminishes beyond 1000 m. They further suggest that the enhancement in power output eventually reaches a saturation point. Complementary to these findings, other researchers have argued that further increases in stack height impose substantial limitations on system performance. Zhou *et al.* [20] report, through theoretical analysis of the MPP, that power output begins to decline when the stack height exceeds 615 m. In their study, the system, which generates ∼45 kW under reference conditions, is shown to achieve a maximum power output of 102.2 kW with increased stack height. Similarly, Karimipour-Fard and Beheshti [14] demonstrate with a 3D CFD study that the maximum power output for the MPP is achieved at a stack height of 685 m, and that power output decreases after this height. Another parameter that plays a key role in system performance, like stack height, is the stack diameter. Air is discharged through the chimney, which, before discharge, rotates the wind turbine at a certain height above the ground, enabling power output. The chimney diameter directly affects the air flow rate discharged from the system, thus impacting system performance. Researchers quantify the effect of chimney diameter on the operational performance of the system in various ways. Because systems with different diameters are difficult to establish experimentally, theoretical and CFD studies are predominantly conducted [2]. When researchers analyse power output for different chimney diameter values for SCPPs, they claim that the chimney diameter range is optimal. Yapıcı *et al.* [21] conduct a geometric analysis for a small-scale system using CFD. The study emphasizes that the chimney diameter should be within a certain range for maximum power output. Toghraie *et al.* [19] investigate the influence of stack diameter on system performance using a three-dimensional CFD model configured with a 100-m stack height and a 100-m collector radius. Their findings indicate

that as the stack radius increases from 1 to 5 m, the power output correspondingly rises; however, beyond this range, further increases in stack radius give rise to a decline in power generation. Similarly, Hamdan [22] performs a theoretical geometric analysis of a large-scale SCPP featuring a 1000-m stack height and a 2000-m collector diameter. The results show that enlarging the stack diameter from 20 to 40 m enhances the power output to ∼13 MW, while additional increases in diameter yield negligible improvements. Collectively, studies in the literature suggest the existence of an optimal range for chimney diameter to achieve maximum performance, a trend that aligns with observations made for the MPP. Recent experimental–numerical studies further reinforce that the relationship between geometric parameters and power output is direct, while system efficiency is simultaneously influenced by solar radiation intensity and ambient temperature variations [23]. Karimipour-Fard and Beheshti [14], in their study based on the MPP, claim that a 12-m chimney diameter will yield 25% more power output than a reference 10-m throat diameter. Chimney height and chimney diameter are critical to the system, and they are two geometric parameters that directly affect system performance. Optimizing these parameters improves system performance while also considering cost. A doubling of chimney height may not be practical because it does not have a positive cost impact on power output. Furthermore, the safety risks associated with an increase in chimney height may also be disadvantageous in this case. Similarly, a similar interpretation can be made for this situation, as an increase in chimney diameter requires more material. Chimney geometry is as critical as its design. An evaluation of the chimney design reveals that the first prototype, Manzanares, has featured a cylindrical chimney design, and later researchers have conducted performance analyses for systems with cylindrical chimney designs [24]. Various studies on chimneys have evaluated the effects of differences in chimney inlet and chimney outlet diameters on the system in different ways. Motoyama *et al.* [25] observe the effects of convergent and divergent chimney designs on system outputs using small-scale prototypes they built in a laboratory environment. They claim that system performance increases in divergent chimney designs, i.e. designs where the chimney outlet area is larger than the chimney inlet area. Similarly, in a different study, Ohya *et al.* [26] experimentally demonstrate that the divergent chimney design offers better performance than the cylindrical chimney design. Sing *et al.* [27] design a small-scale system using a two-dimensional axisymmetric CFD model and analyse the divergent chimney design and chimney height together. They validate the model with experimental data and claim that the MPP, which traditionally produces a power output of 50 kW, might produce a power output of 1738 kW. Studies on chimney design are more limited in the literature than those on chimney height and diameter, and it is understood that there are different interpretations among researchers. Researchers generally agree that the divergent chimney design provides better performance, particularly for the MPP [2]. However, there is no clear consensus on the ratio of the chimney exit area to the chimney inlet area (AR). Araya and Teferi [28] review various studies concerning chimney design in SCPPs and highlight the absence of a unified consensus within the literature. Adibimanesh *et al.* [29] investigate the impact of divergent chimney configurations on SCPP performance through the development of a two-dimensional axisymmetric CFD model. Using the geometry of the MPP as a reference, they compare the baseline configuration with AR of 3.72 and 8.37 by employing the Response Surface Method. Their findings indicate that, at an AR of 8.37, the pressure potential increases from 66.1 to 332.6 Pa, while the mass flow rate rises from 901 to 2008 kg/s. More recent geometry-oriented numerical studies demonstrate that nonuniform or stepped chimney configurations can further enhance pressure recovery, airflow uniformity, and energy efficiency without relying on dimensional scaling, thereby highlighting the importance of advanced geometry optimization strategies [30]. A comparative summary of performance data from studies analysing divergent chimney designs based on the MPP is provided in Table 2.

SCPPs are large-scale systems characterized by extensive collector areas and tall chimneys. Consequently, scaling up the collector size or chimney height to enhance system performance often results in substantially higher investment costs, construction complexity, and safety risks. Therefore, performance improvement through geometry-oriented design adjustments rather than dimensional scaling is of particular practical interest. However, the literature still lacks a unified assessment of (i) the optimal chimney diameter range and (ii) the optimal divergent chimney configuration [i.e. chimney exit-to-inlet area ratio (AR)] for large-scale reference systems such as the MPP, and these two geometric effects are frequently analysed separately, which limits design-level conclusions. To address this gap, the present study employs a validated three-dimensional CFD framework to systematically quantify the coupled influence of chimney diameter variation and divergent chimney design on MPP performance under identical reference conditions. The optimum chimney diameter and the permissible ranges beyond which performance deterioration occurs are identified. Moreover, the study clarifies why chimney divergence is critical to improving pressure potential, mass flow rate, and ultimately power output, and it determines the corresponding maximum performance operating ranges. The remainder of this paper is organized as follows: Section 2 describes the numerical model, governing equations, boundary conditions, and validation procedure; Section 3 presents and discusses the CFD results for different chimney diameters and AR values; Section 4 provides the optimization-based design implications; and Section 5 summarizes the main conclusions and outlines recommendations for future SCPP development.

2. Materials and methods

This study, based on the MPP, analyses the stack sizing and design for SCPPs by conducting a CFD analysis using a dimensionless stack diameter and a divergent stack design. Initially, during the model creation phase, the 3D model includes two plane symmetries at 90°. The use of a 90° symmetry sector significantly reduces computational cost whilst preserving the essential flow physics of the full-scale system, as commonly adopted in large-scale SCPP simulations. The analysis includes several fundamental assumptions regarding the air density within the system, airflow characteristics, and the analysis, including the following:

- Air is assumed to be incompressible. This assumption is justified since the maximum airflow velocities remain well below the compressibility limit and the temperature rise within the system is limited, allowing density variations to be accurately captured via buoyancy modelling. In all solutions,

Table 2 Divergent chimney configurations and corresponding performance data reported for the MPP.

Reference	Reference results[a] V_{max} (m/s)	Power output (kW)	AR	Divergent chimney results V_{max} (m/s)	Power output (kW)
[31]	–	34.087	9	–	83.47
[32]	15.1	50.37	10	–	680
[33]	9.1	33.7	1.66	11.615	70.1
[34]	9.1	37.084	1.7	11.7	71.52
[35]	10.57[b]	51.59	2.25	19	75.91
[36]	–	19.5	8.7	28.8	231.7
[16]	14.2	54.3	3.5	19.4	168.5
[37]	15	–	3.5	50.5	–

[a]Cylindrical chimney design. [b]Velocity at chimney inlet.

Table 3 Parameters and calculated values used in the evaluation of the RA.

Parameter	g (m/s^2)	β (1/K)	ΔT	H_{coll} (m)	α (m^2/s)	ν (m^2/s)
Value	9.81	0.00333	20	1.85	2.044×10^{-5}	1.521×10^{-5}

the momentum, energy, and continuity equations are solved simultaneously using ANSYS FLUENT and are given in Eqs (1)–(3), respectively [38]:

$$\frac{\partial}{\partial t}\left(\rho.\vec{v}\right)+\nabla\left(\rho.\vec{v}.\vec{v}\right)= -\nabla p+.\left(\mu\left[\left(\nabla\vec{v}+\nabla\vec{v}^{T}\right)-\frac{2}{3}\nabla.\vec{v}I\right]\right)+\rho\{\vec{g}\} \quad (1)$$

$$\frac{\partial}{\partial t}(\rho E)+\nabla.\left(\vec{v}\,(\rho E+p)\right)= \nabla.\left(k_{eff}\nabla T-h\vec{j}+\left(\mu\left[\left(\nabla\vec{v}+\nabla\vec{v}^{T}\right)-\frac{2}{3}\nabla.\vec{v}I\right].\vec{v}\right)\right) \quad (2)$$

$$\frac{\partial\rho}{\partial t}+\nabla.\left(\rho.\vec{v}\right)=0 \quad (3)$$

- The flow regime is assumed to be steady and turbulent from the system inlet to the outlet. This is because the turbulence limit is exceeded in the calculation of the Rayleigh number (Ra), which determines the flow characteristics for natural convection. The calculation details are stated in Eq. (4) [39]:

$$\mathrm{Ra}=\frac{g\beta\Delta T{H_{\mathrm{coll}}}^{3}}{\alpha\vartheta} \quad (4)$$

where g represents the gravitational acceleration, β the thermal expansion coefficient, ΔT the temperature difference, H_{coll} the collector height, α the thermal diffusivity coefficient, and ν the kinematic viscosity. Turbulent flow is assumed because the Ra number in the system is greater than 10^{10} [40]. Calculation details are given in Table 3.

Since the Ra exceeds the turbulent regime limit, the flow is treated as turbulent. Assuming constant air viscosity, the transport equations of the Standard k-ε turbulence model are solved using Eqs (5) and (6) [41]:

$$\frac{\partial(\rho k)}{\partial t}+\frac{1}{r}\frac{\partial}{\partial r}(\rho rku)+\frac{\partial(\rho k\nu)}{\partial y}=\frac{1}{r}\frac{\partial}{\partial r}\left[r\left(\mu+\frac{\mu_t}{\sigma_k}\right)\frac{\partial k}{\partial r}\right]+\frac{\partial}{\partial y}\left[\left(\mu+\frac{\mu_t}{\sigma_k}\right)\frac{\partial k}{\partial y}\right]+G_k+\beta g\frac{\mu_t}{\mathrm{Pr}_{kt}}\frac{\partial T}{\partial y}-\rho\epsilon \quad (5)$$

$$\frac{\partial(\rho\varepsilon)}{\partial t}+\frac{1}{r}\frac{\partial}{\partial r}(\rho r\varepsilon u)+\frac{\partial(\rho\varepsilon\nu)}{\partial y}=\frac{1}{r}\frac{\partial}{\partial r}\left[r\left(\mu\frac{\mu_t}{\sigma_\varepsilon}\right)\frac{\partial\varepsilon}{\partial r}\right]+\frac{\partial}{\partial y}\left[\left(\mu+\frac{\mu_t}{\sigma_\varepsilon}\right)\frac{\partial\varepsilon}{\partial y}\right]+G_kC_{1\varepsilon}\left(\frac{\varepsilon}{k}\right)-C_{2\varepsilon}\rho\left(\frac{\varepsilon^2}{k}\right) \quad (6)$$

The constants for Eqs (5) and (6) are listed in Eq. (7):

$$C_{1\varepsilon}=1.44, C_{2\varepsilon}=1.92, \sigma_\varepsilon=1.3, \sigma_k=1.0 \quad (7)$$

- Climatic parameters are assumed to remain constant throughout the analysis. The system is based on a solar irradiance of 1000 W/m^2 and an ambient temperature of 300 K, which are clearly stated in experimental data and widely used in the literature [2].
- The temperature change of air is limited. Experimental data indicate that the temperature change in the system is 20 K [6]. Therefore, the density of air is evaluated using the Boussinesq approximation, as given in Eq. (8) [42]:

$$(\rho-\rho_a)\,g=\rho_a\beta\,(T-T_a) \quad (8)$$

The 3D CFD model designed in the model creation phase, the first step of the analysis, and the schematic view of the geometric details of the chimney diameter and divergent chimney design to be analysed in the study are shown in Fig. 1. The dimensioning of the system is based on the reference geometry established by Haaf *et al.* [43]. In the analysis of chimney configurations, the evaluation is conducted by comparing various chimney diameters to the

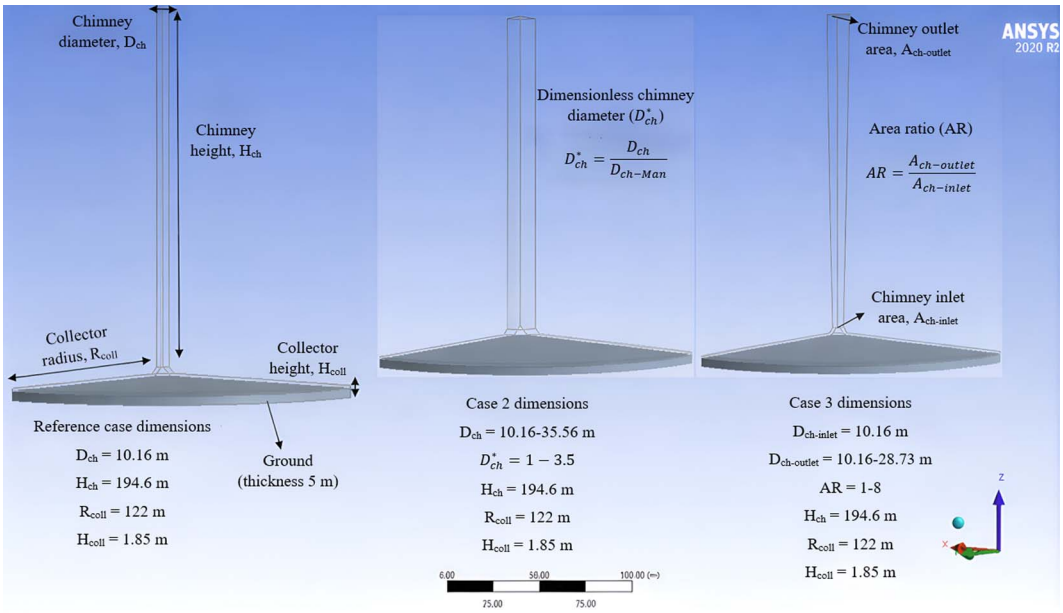

Figure 1 Three-dimensional CFD model illustrating the investigated chimney diameter configurations and divergent chimney design, along with their corresponding images and technical specifications.

reference system, employing a dimensionless chimney diameter for consistency. For divergent chimney designs, the assessment is carried out using the AR, defined as the ratio between the chimney exit area and the inlet area, which serves as a key parameter influencing flow characteristics and overall system performance.

For the numerical assessments, the chimney is assumed to be constructed from the composite material employed in the reference pilot installation, while the collector cover is modelled using glass, and the ground layer is represented by a soil–gravel composite. Atmospheric air is adopted as the operating fluid within the system. The thermophysical characteristics of all materials considered are summarized in Table 4 [44]. Experimental evidence indicates that subsurface temperature stabilizes beyond a depth of ∼1 m [6]. In light of this observation, a ground domain thickness of 5 m is selected in the present investigation to more accurately capture subsurface heat transfer behaviour and associated thermal interactions. As previously calculated, the flow characteristics of the working fluid, air, are assumed to be turbulent. The flow regime is important in CFD analyses. The student version of the ANSYS engineering simulation programme used in this study has different turbulence preferences in the FLUENT solver. After creating the reference model, it is crucial to select the correct turbulence model. For this purpose, a comparison of different turbulence models is performed. The system outputs for the different turbulence models are given in Table 5. The comparison reveals no significant differences in system outputs due to the varying turbulence models. The maximum airflow velocity for different turbulence models varies between 15.565 and 15.955 m/s. In this case, the variation is limited to 2.4%. Based on this comparison, the Standard k-ε (two-equation) turbulence model is selected due to its computational efficiency, numerical stability, and suitability for buoyancy-driven turbulent flows in large-scale systems. The buoyancy effect is set to full, and viscous heating is enabled. Solar radiation is modelled using the Solar Ray Tracing algorithm within the Discrete Ordinates (DO) radiation model, with the solar ray angle automatically calculated according to the geographical location of the MPP. Pressure–velocity coupling is achieved using the SIMPLE algorithm. PRESTO! is selected for pressure discretization, while second-order upwind schemes are used for the remaining variables. A convergence criterion of 10^{-5} is applied for all residuals. The solution procedure flowchart is shown in Fig. 2, and the boundary conditions and computational mesh are presented in Fig. 3.

The power output calculation procedure used in this study is based on CFD results. Power output (P_o) is determined by two key parameters: volumetric flow rate (Q) and the mean pressure difference (ΔP_{tur}) at the turbine location. The turbine pressure drop coefficient, which determines the turbine's power output potential, is taken from experimental data [6] and is assumed to be 2/3. Finally, the turbine efficiency (η_{tur}) is included in the calculation as 0.8, a value commonly used in the literature. The power output calculation is detailed in Eq. (9):

$$P_o = \frac{2}{3} \times \eta_{tur} \times Q \times \Delta P_{tur} \tag{9}$$

3. Mesh independence test and model validation

In this study, which analyses the stack configuration for SCPPs, the reliability of the first 3D CFD model is tested. For this purpose, a mesh-independent solution and validation steps are performed. For the mesh-independent solution, air velocities at 1 m above the ground level under the collector are compared along the collector with different minimum cell sizes. The graph of the comparison for minimum element sizes of 0.7, 0.8, 0.9, and 1 m is shown in Fig. 4. The cell numbers are also included in the graph. An examination of the graph reveals that the air flow velocity under the collector does not change significantly with different cell numbers. In this case, 658 234 cells are deemed sufficient for the solutions. Following

Table 4 Thermophysical properties of materials used in the CFD simulations [45, 46].

Material	Density (kg/m ^{3})	Specific heat capacity (J/kg K)	Thermal conductivity (W/m K)	Thickness (m)
Chimney	2100	880	1.4	0.00125
Ground	2160	710	1.84	5
Glass	2500	750	1.15	0.004

Table 5 System outputs for different turbulence models.

Turbulence model/system output	Maximum velocity (m/s)	Mass flow rate (kg/s)	Power output (kW)
Standard k-ε	15.565	1141.388	55.885
RNG k-ε	15.955	1152.876	57.86
Realizable k-ε	15.76	1164.248	59.93
Standard k-ω	15.955	1162.698	59.339
GEKO k-ω	15.817	1166.728	60.054
BSL k-ω	15.878	1173.34	60.986
SST k-ω	15.877	1166.876	60.06

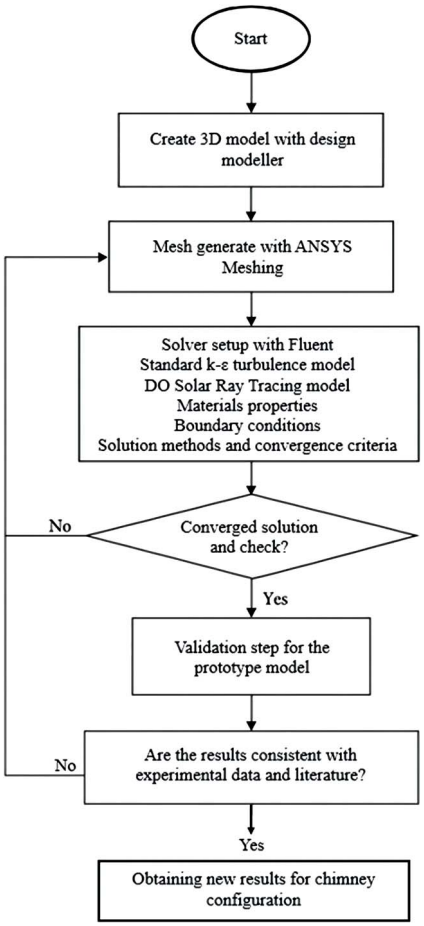

Figure 2 CFD solution procedure adopted in the present study.

the attainment of a mesh-independent solution, the subsequent validation stage is conducted to verify the accuracy and reliability of the CFD simulation results. In the validation step, multifaceted verification is performed, and comparisons are made with both experimental data and similar studies in the literature to ensure high reliability. First, the maximum air velocity and power output within the system are used for comparison with the experimental data [47]. Details of the comparison are provided in Table 6. Experimental data are based on real-time measurements. CFD solutions are obtained under steady-state conditions. Therefore, it is a natural expectation that the system performance will be higher under steady-state conditions. Comparison with similar CFD studies in the literature reveals results that parallel experimental data. Secondly, the validation phase relies on similar studies in the literature. Air velocity is compared under the collector at a height of 0.85 m above the ground. The comparison graph for 750 W/m^2 solar irradiance and 300 K ambient temperature is presented in Fig. 5. An analysis of the graph indicates that the CFD results exhibit strong agreement with those reported in comparable studies within the existing literature.

4. Results and discussion

After completing the mesh-independent solution and verification steps of the CFD model, the results are analysed by first examining the reference configuration of the MPP, followed by a systematic evaluation of chimney diameter and divergent chimney design effects. Due to the semitransparent nature of the collector, incoming solar radiation penetrates the collector cover and is absorbed at the ground level, leading to a rise in ground temperature [49]. As a result, the air beneath the collector is heated and progressively accelerates towards the chimney inlet, as illustrated in Figs 3 and 4. The rise in air velocity in this region enhances convective heat transfer from the ground surface. Consequently, a reduction in ground temperature is anticipated near the chimney inlet. For the reference configuration, under a solar irradiance of 1000 W/m^2 and an ambient temperature of 300 K, Fig. 6 presents the temperature distribution along the plane of symmetry as well

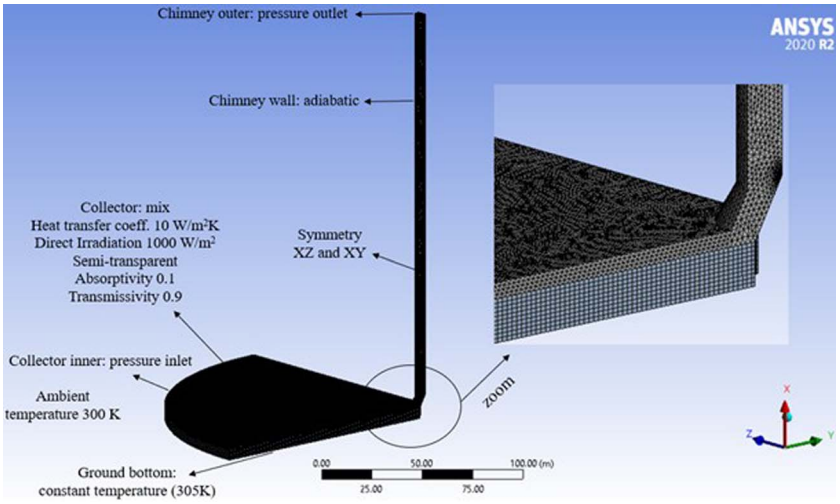

Figure 3 Computational domain, boundary conditions, and mesh structure used in the CFD simulations.

Table 6 Comparing the CFD result with experimental results and similar studies in the literature for model validation.

	Maximum air velocity (m/s)	Power output (kW)	Rate of mass flow (kg/s)
Experimental results [47]	15	50	–
CFD results	15.565	55.885	1141.388
% change	3.76	11.77	–
Similar study [48]	14.9	46	1018.6

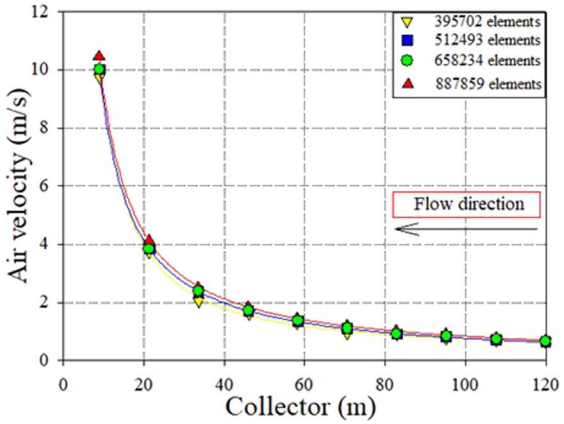

Figure 4 Air velocity distribution beneath the collector obtained with different mesh resolutions.

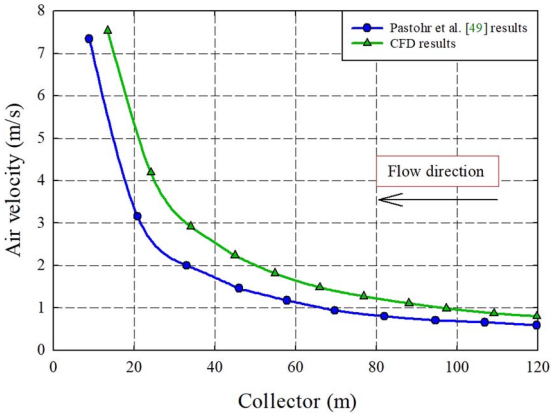

Figure 5 Comparison of the airflow velocity predicted in the present study with experimental and numerical data reported in the literature.

as the ground-level temperature profile. A pronounced decrease in ground temperature is observed near the chimney inlet, consistent with the locally intensified airflow. The maximum ground temperature predicted by the CFD model reaches 376 K. Experimental data indicate that the maximum temperature measured at the centre of the collector at the ground level is ∼345 K [6]. This discrepancy can be attributed to the steady-state nature of the CFD simulations and the spatial limitations of experimental measurements. Comparable ranges for maximum ground temperature have also been reported in the literature, with values between 370 K [50], while others claim that it will be 390 K [51].

From a physical perspective, the coupled temperature and velocity fields beneath the collector are governed by buoyancy-driven natural convection. Heating of the air near the ground reduces its density, generating an upward buoyant force that accelerates the flow towards the chimney inlet. This mechanism simultaneously increases air velocity and convective heat transfer, thereby explaining the observed reduction in ground temperature close to the chimney entrance. This behaviour establishes the chimney as the primary driving component of the system and motivates the subsequent geometric optimization analyses. After discussing the results from the reference case, the chimney configuration, which is the driving force of the system, is

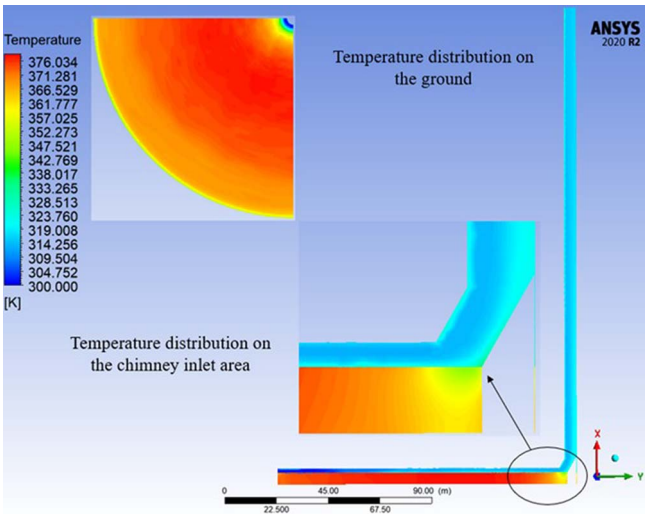

Figure 6 Temperature field inside the system and ground surface temperature distribution for the reference configuration at 1000 W/m^2 solar irradiance and 300 K ambient temperature.

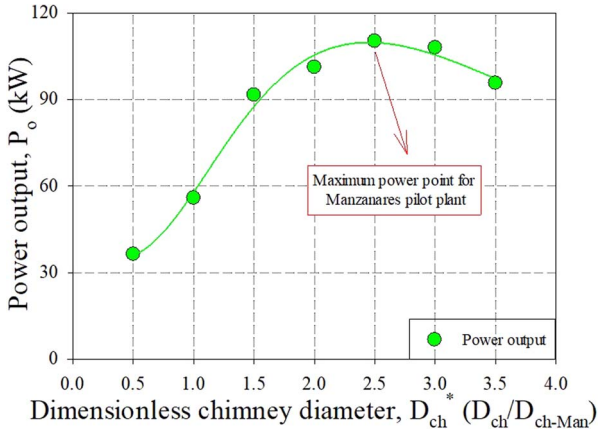

Figure 7 Graph of power output versus different dimensionless chimney diameters.

discussed. In the reference case, the chimney diameter for the MPP is 10.16 m. To analyse the chimney diameter over a wide range, the chimney diameter is first halved. It is then increased by a factor of 3.5, and the system outputs are examined for values within this range. The variation of power generation with respect to the dimensionless chimney diameter is illustrated in Fig. 7. The results demonstrate a clear nonlinear relationship between chimney diameter and power output. Starting from the reference case, increasing the chimney diameter initially leads to a substantial enhancement in power output, reaching a maximum value exceeding 110 kW, corresponding to an increase of ∼97%. Beyond this point, further increases in chimney diameter result in a decline in power output, indicating the existence of an optimal diameter range. For the MPP, this optimal range lies between 20.32 and 30.48 m. A detailed quantitative assessment of the underlying flow parameters is provided in Table 7, which summarizes the variations in maximum airflow velocity, mass flow rate, and average pressure difference at the turbine location for different dimensionless chimney diameters. As shown in Table 7, increasing chimney diameter leads to a substantial rise in mass flow rate due to the enlarged flow cross-section. When the chimney diameter is tripled relative to the reference configuration, the mass flow rate increases by nearly three-fold. In contrast, the mean pressure difference at the turbine location decreases monotonically with increasing chimney diameter. This coupled behaviour explains the nonlinear variation of power output. When the chimney diameter is reduced to half of the reference value, the average pressure difference at the turbine location approximately doubles; however, the mass flow rate decreases by 68.06%, resulting in a net reduction in power output. At a chimney diameter of 25.4 m, corresponding to the maximum power output condition, the mass flow rate increases to 2916.02 kg/s, representing a 155.48% increase compared to the reference case, while the power output boosts by only a factor of two due to the simultaneous reduction in pressure difference across the turbine. These results demonstrate that chimney diameter governs system performance through a trade-off between mass flow rate and pressure potential. Whilst larger diameters enhance airflow, excessive enlargement weakens the buoyancy-induced pressure difference driving the system. This interaction gives rise to a well-defined optimal chimney diameter for maximum power generation. The observed trends are consistent with findings reported in the literature. Previous studies based on the MPP and other SCPP configurations similarly identify an optimal chimney diameter when other geometric parameters are held constant. A comparative summary of these studies is presented in Table 8.

Table 8 highlights that the optimal chimney diameter range reported in the literature varies considerably, even for studies based on the MPP. The present study identifies an optimal range of ($D_{ch}/D_{ch\text{-}ref}$ = 2–3), which is lower than the values reported in some previous MPP-based investigations, such as the range of 4.5–5 reported in Ref. [52]. This discrepancy can be attributed primarily to differences in modelling assumptions and boundary condition definitions. Studies predicting larger optimal diameters often impose simplified thermal boundary conditions, such as prescribing a constant heat flux at the ground level, which can overestimate buoyancy-induced pressure potential and favour larger chimney cross-sections. In contrast, the present study explicitly models solar radiation and buoyancy-driven heat transfer within a fully three-dimensional CFD framework, leading to a more realistic prediction of airflow acceleration and pressure development. Similarly, studies reporting relatively modest performance enhancements, such as the 3.5% increase reported in Ref. [14], typically investigate a narrower diameter range or operate under more constrained geometric conditions. When compared with studies that report power increases of 60%–66% [12, 53], the 97% power enhancement obtained in the present work reflects both the wider parametric range considered and the more comprehensive physical representation of the system. Overall, these comparisons indicate that whilst the existence of an optimal chimney diameter is a consistent finding across the literature, its exact value is highly sensitive to the adopted modelling strategy and thermal boundary conditions.

While increasing chimney diameter can nearly double the power output relative to the reference configuration, further enlargement raises concerns related to construction cost and structural safety. Therefore, the second part of the analysis focuses on chimney geometry optimization through the adoption of a divergent chimney design, in which the chimney inlet area is kept constant, and the exit area is increased. The effect of

Table 7 Airflow velocity, mass flow rate, and average pressure difference at the turbine location for different dimensionless chimney diameters.

$D_{ch}/D_{ch\text{-}Man}$	Maximum velocity (m/s)	Rate of mass flow (kg/s)	Pressure difference at turbine location (Pa)
0.5	23.26	364.464	220.174
1 (reference case)	15.565	1141.388	107.963
1.5	15.848	2187.016	92.429
2	16.163	2747.12	81.282
2.5	15.75	2916.02	76.771
3	14.509	3340.444	71.305
3.5	13.356	3558.148	59.919

Table 8 Performance characteristics reported in the literature for different chimney diameter configurations.

Reference	Geometric details	Optimum performance range ($D_{ch}/D_{ch\text{-}ref}$)	Power output details
Present study	MPP	2–3	The power output shows a 97% increase compared to the reference case, reaching a value of 110 kW
[52]	MPP	4.5–5	Maximum power output 209 kW for optimum chimney diameter
[14]	MPP	1.08–1.28	For a chimney diameter of 12.6 m, the power output exhibits a 3.5% increase relative to the reference configuration
[12]	MPP	–	At a chimney diameter of 30 m, the power output increases by 60.29% relative to the reference case, reaching a value of 82.575 kW
[19]	100-m chimney height, 200-m collector diameter, and 8-m chimney diameter	1–1.5	When the chimney diameter is 10 m, the power output increases by 8.9% to 85.8 kW
[53]	1000-m chimney height, 4300-m collector diameter, and 110-m chimney diameter	2.76–3.5	When the chimney diameter is 350 m, the power output increases by 65.9% to 146 MW

divergent chimney geometry is quantified using the chimney exit-to-inlet AR. Figure 8 presents the variation of power output with AR under identical geometric and climatic conditions. Among all investigated configurations, the divergent chimney design exhibits the most pronounced performance enhancement. Power output increases sharply with AR and reaches a maximum value of ∼369.4 kW at an AR of 4, corresponding to a 5.5-fold increase compared to the reference cylindrical chimney. Beyond AR = 5, power output declines rapidly, while further increases beyond AR = 6 lead to only marginal additional reductions. The superior performance of the divergent chimney design is attributed to pressure recovery within the expanding flow passage. A gradual increase in cross-sectional area converts kinetic energy into static pressure, thereby enhancing the pressure difference across the turbine. At moderate AR values, particularly around AR = 4, the expansion angle remains sufficiently small to prevent flow separation, allowing efficient pressure recovery. For larger AR values, excessive expansion leads to boundary layer separation and increased aerodynamic losses, which diminish pressure recovery and reduce power output. At the optimal AR value of 4, the maximum air velocity increases from 15.565 m/s in the reference case to 28.671 m/s, while the mass flow rate rises from 1141.488 to 2137.832 kg/s. Simultaneously, the mean pressure difference at the turbine location increases from 107.963 to 380.997 Pa. Beyond this optimal point, all three parameters decrease. At AR = 8, the maximum air velocity drops to 25.056 m/s, the mass flow rate decreases to 1860.492 kg/s, and the average pressure difference reduces to 306.645 Pa, confirming the existence of an optimal divergent chimney configuration.

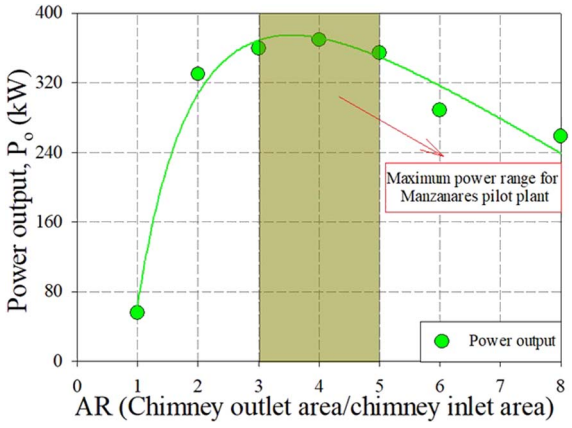

Figure 8 Power output as a function of the chimney exit-to-inlet AR.

Various studies on chimney design are available in the literature. Researchers analyse system performance using the AR value or chimney divergence angle, keeping the chimney inlet area constant. A comparison of the current study and other studies in the literature is presented in Table 9. It clearly shows that the reported performance enhancement associated with divergent chimney designs varies over a wide range, even when the MPP is used as the reference system. The present study predicts a 5.6-fold increase in power output at an optimal AR value of 4, which is higher than the improvements reported in several earlier studies that employ relatively small divergence angles and simplified modelling approaches, such as the two-dimensional analyses reported in Refs [31, 54]. These studies typically yield modest to moderate performance gains, partly because two-dimensional formulations cannot fully capture three-dimensional flow separation, pressure recovery, and turbulence effects within the expanding chimney section. On the other hand, studies reporting very large enhancements, including the 11.9-fold increase claimed in Ref. [36], generally adopt higher AR values and operate under different climatic conditions and boundary assumptions. In such cases, the combination of reduced ambient temperature and elevated buoyancy potential can amplify pressure recovery within the chimney, leading to significantly larger predicted power outputs. The present study yields a lower, but more conservative and physically plausible, performance enhancement by explicitly modelling solar radiation, buoyancy-driven turbulence, and three-dimensional flow expansion under standard reference conditions (1000 W/m^2, 300 K). Importantly, the close agreement between the maximum air velocity predicted in the present study (28.671 m/s at AR = 4) and the value reported in Ref. [36] (28.9 m/s) indicates that the dominant flow physics is captured consistently, despite differences in predicted power output.

5. Conclusions

SCPPs offer the potential to produce electricity directly from solar energy, and their simple structure and operating principle are noteworthy. This study provides a detailed analysis of the chimney, which is critical for the system's first application, the MPP. Although chimney height has been extensively examined in the literature and its performance implications are relatively well established, the combined effects of chimney diameter optimization and divergent chimney design have not been systematically analysed for large-scale reference systems. A validated three-dimensional CFD model based on the MPP geometry is developed and benchmarked against experimental measurements and published numerical studies. Simulations are performed under reference conditions of 1000 W/m^2 solar irradiance and an ambient temperature of 300 K. The main findings and contributions of the study can be summarized as follows:

- The 90° three-dimensional CFD model offers a computationally efficient approach while yielding results that demonstrate strong consistency with both experimental findings and previously reported data in the literature.
- A detailed mesh independence study and multilevel validation confirm the robustness and reliability of the CFD framework for large-scale buoyancy-driven solar chimney flows.
- Comparative evaluation of commonly used turbulence models reveals negligible differences in predicted airflow and power output, indicating that system-level performance predictions are weakly sensitive to turbulence model selection under the investigated conditions.
- Under 1000 W/m^2 solar irradiance and an ambient temperature of 300 K, the reference cylindrical chimney configuration produces a power output of 55.885 kW, which shows close agreement with the experimentally reported value of ∼50 kW for the MPP.
- The chimney diameter is critical to the system. Increasing the chimney diameter by 2.5 times the reference value increases power output by 97%, reaching 110 kW. However, increasing the chimney diameter further has a negative impact on power output.
- Quantitative analysis reveals that the nonlinear variation of power output with chimney diameter arises from the coupled interaction between mass flow rate and buoyancy-induced pressure difference, highlighting the existence of a well-defined optimal diameter range for maximum power generation.
- Divergent chimney design is shown to be one of the most effective configuration parameters for improving system performance. An optimal AR of 4 yields a maximum power output of ∼369.4 kW, representing a 5.6-fold increase compared to the reference cylindrical configuration, whereas larger AR values result in performance degradation.
- At the optimal divergent configuration, the maximum air velocity increases from 15.565 to 28.671 m/s, the mass flow rate rises from 1141.5 to 2137.8 kg/s, and the mean pressure difference at the turbine increases from 107.96 to 380.99 Pa, collectively explaining the observed multifold power enhancement.
- Beyond the optimal AR value, further increases in chimney divergence result in reduced power output due to flow separation and increased aerodynamic losses, clearly defining practical design limits for divergent chimney implementation.

The key novelty of this study lies in demonstrating that multifold performance enhancement in a large-scale SCPP can be achieved through aerodynamic optimization of chimney geometry alone, without any increase in chimney height. Unlike previous studies that primarily rely on structural scaling or isolated geometric modifications, the present work provides a validated, output-oriented design framework showing that the coupled optimization of chimney diameter and divergent geometry can effectively compensate for height limitations. Several limitations of the present study should be acknowledged. The simulations are conducted under steady-state conditions and assume constant climatic parameters, representing peak operating conditions but not capturing transient diurnal behaviour. In addition, turbine performance is represented using fixed efficiency and pressure-drop coefficients, and blade-resolved aerodynamic effects are not explicitly modelled. Structural feasibility, economic cost, and material constraints associated with large divergent chimney geometries are also beyond the scope of the present analysis. Future studies will analyse whether systems with different heights, in addition to chimney diameter and divergent chimney design, can achieve greater power output from a system with a lower chimney height than the reference value. The current study results indicate that

Table 9 SCPPs performance analysis and technical details through divergent chimney design on MPP.

Ref.	Study details	Climatic details	Optimum divergent chimney angle or AR value	Power output details
Present study	Divergent chimney effect is analysed based on 3D CFD model.	1000 W/m^2 and 300 K	4 AR value	The power output increases by a factor of 5.6 compared to the reference configuration, reaching a value of 369.4 kW
[54]	The influence of the divergent chimney configuration is investigated through a two-dimensional CFD analysis	960 W/m^2 and 302 K	1.43 divergent chimney angle	Power output increased by 3.18% to 51 kW
[35]	They evaluate the effect of the chimney divergence angle on the system performance with a 3D CFD model	1000 W/m^2 and 302 K	0.75 divergent chimney angle	The power generation exhibits a 47% enhancement relative to the baseline condition, attaining a value of 76 kW
[31]	The influence of the chimney divergence angle on system performance parameters is examined through a two-dimensional CFD analysis	800 W/m^2 and 300 K	3 divergent chimney angles	Power output is shown to be 83.47 kW, an increase of 145.5% compared to the pilot case
[33]	Divergent chimney performance is evaluated by creating a 3D CFD model	The Manzanares location is referenced to a typical June day at 1:00 pm	1 divergent chimney angle	Power output is claimed to be ∼70 kW, an increase of 108% compared to the reference case
[36]	The divergent chimney effect is interpreted with a 3D CFD model	850 W/m^2 and 296.65 K	8.7 AR value	Power output is claimed to increase by 11.9 times to 231.7 kW

different designs, particularly those with divergent chimney designs, can increase power output while reducing system size.

Acknowledgements

The authors extend their appreciation to the Deanship of Research and Graduate Studies at King Khalid University for funding this work through Large Research Project under grant number RGP.2/387/46.

Author contributions

Pinar Mert Cuce (Methodology [equal], Software [equal], Visualization [equal], Writing—original draft [equal], Writing—review & editing [equal]), Erdem Cuce (Conceptualization [equal], Investigation [equal], Supervision [equal], Validation [equal], Writing—original draft [equal], Writing—review & editing [equal]), Saad Alshahrani (Conceptualization [equal], Funding acquisition [equal], Visualization [equal], Writing—review & editing [equal]).

Conflicts of interest

The authors declare that they have no known competing financial interests or personal relationships that could have appeared to influence the work reported in this paper.

Funding

None declared.

Data availability

Data available on request from the authors.

References

1. He R, Luo L, Shamsuddin A. *et al.* Corporate carbon accounting: a literature review of carbon accounting research from the Kyoto Protocol to the Paris Agreement. *Account Finance* 2022;**62**:261–98. https://doi.org/10.1111/acfi.12789.
2. Cuce E. Dependence of electrical power output on collector size in Manzanares solar chimney power plant: an investigation for thermodynamic limits. *Int J Low-Carbon Technol* 2022;**17**:1223–31. https://doi.org/10.1093/ijlct/ctac094.
3. Cuce E, Bali T. 19-23 April 2009. Variation of cell parameters of a p-Si PV cell with different solar irradiances and cell temperatures in humid climates. In *Fourth International Exergy, Energy and Environment Symposium*. Sharjah, United Arab Emirates.
4. Ahmadi MH, Ghazvini M, Sadeghzadeh M. *et al.* Solar power technology for electricity generation: a critical review. *Energy Sci Eng* 2018;**6**:340–61. https://doi.org/10.1002/ese3.239.
5. Cuce E. Divergent chimney and sloping collector design for ground heat source integrated solar chimney power plants. *J Therm Anal Calorim* 2024;**149**:14147–61. https://doi.org/10.1007/s10973-024-13669-5.
6. Haaf W. Solar chimneys: part ii: preliminary test results from the MPP. *Int J Sustain Energy* 1984;**2**:141–61.
7. Biswas N, Mandal DK, Bose S. *et al.* Experimental treatment of solar chimney power plant—a comprehensive review. *Energies* 2023;**16**:6134. https://doi.org/10.3390/en16176134.

8. Al-Ghezi MK, Ashour AM, Ali Kadhim S. *et al.* Influence study of different types of grounds on the solar chimney power plant performance. *Energy Sources A Recovery Util Environ Eff* 2025;**47**:6976–95. https://doi.org/10.1080/15567036.2025.2477836.
9. Behera BK, Sahoo SS, Kumar S. Technology, design, and performance of solar chimney power plants: an updated and thorough review. *Int J Green Energy* 2025;**22**:1816–49. https://doi.org/10.1080/15435075.2024.2446492.
10. Cuce E, Cuce PM, Sen H. A thorough performance assessment of solar chimney power plants: case study for Manzanares. *Cleaner Eng Technol* 2020;**1**:100026. https://doi.org/10.1016/j.clet.2020.100026.
11. Cuce E, Sen H, Cuce PM. Numerical performance modelling of solar chimney power plants: influence of chimney height for a pilot plant in Manzanares, Spain. *Sustain Energy Technol Assess* 2020;**39**:100704. https://doi.org/10.1016/j.seta.2020.100704.
12. Ikhlef K, Larbi S. 2019. Energy performance analysis of a solar chimney power plant with and without thermal storage system. In *6th International Conference on Automation, Control, Engineering and Computer Science ACECS*, Vol. **11**. İstanbul, Turkey. 1–7.
13. Li JY, Guo PH, Wang Y. Effects of collector radius and chimney height on power output of a solar chimney power plant with turbines. *Renew Energy* 2012;**47**:21–8. https://doi.org/10.1016/j.renene.2012.03.018.
14. Karimipour-Fard P, Beheshti H. Performance enhancement and environmental impact analysis of a solar chimney power plant: twenty-four-hour simulation in climate condition of Isfahan province, Iran. *Int J Eng* 2017;**30**:1260–9.
15. Semai H, Bouhdjar A, Larbi S. Canopy slope effect on the performance of the solar chimney power plant. *Int J Green Energy* 2017;**14**:229–38. https://doi.org/10.1080/15435075.2016.1253580.
16. Cuce E, Saxena A, Cuce PM. *et al.* Performance assessment of solar chimney power plants with the impacts of divergent and convergent chimney geometry. *Int J Low-Carbon Technol* 2021;**16**:704–14. https://doi.org/10.1093/ijlct/ctaa097.
17. Ayadi A, Driss Z, Bouabidi A. *et al.* A computational and an experimental study on the effect of the chimney height on the thermal characteristics of a solar chimney power plant. *Proc Inst Mech Eng E: J Process Mech Eng* 2018;**232**:503–16. https://doi.org/10.1177/0954408917719776.
18. Kasaeian A, Ghalamchi M, Ghalamchi M. Simulation and optimization of geometric parameters of a solar chimney in Tehran. *Energ Conver Manage* 2014;**83**:28–34. https://doi.org/10.1016/j.enconman.2014.03.042.
19. Toghraie D, Karami A, Afrand M. *et al.* Effects of geometric parameters on the performance of solar chimney power plants. *Energy* 2018;**162**:1052–61. https://doi.org/10.1016/j.energy.2018.08.086.
20. Zhou X, Yang J, Xiao B. *et al.* Analysis of chimney height for solar chimney power plant. *Appl Therm Eng* 2009;**29**:178–85. https://doi.org/10.1016/j.applthermaleng.2008.02.014.
21. Yapıcı EO, Ayli E, Nsaif O. Numerical investigation on the performance of a small scale solar chimney power plant for different geometrical parameters. *J Clean Prod* 2020;**276**:122908. https://doi.org/10.1016/j.jclepro.2020.122908.
22. Hamdan MO. 2010. Analytical thermal analysis of solar chimney power plant. In *4th International Conference on Energy Sustainability*, Vol. **43949**. Phoenix, Arizona, USA. 451–5.
23. Al-Ghezi MK, Kadhim SA, Rashid FL. Numerical and experimental analyses of solar chimney parameters. *J Sol Energy Eng* 2025;**147**:051006. https://doi.org/10.1115/1.4068682.
24. Schlaich J. *The Solar Chimney: Electricity from the Sun*. Edition Axel Menges, 1995.
25. Motoyama M, Sugitani K, Ohya Y. *et al.* Improving the power generation performance of a solar tower using thermal updraft wind. *Energy Power Eng* 2014;**06**:362–70. https://doi.org/10.4236/epe.2014.611031.
26. Ohya Y, Wataka M, Watanabe K. *et al.* Laboratory experiment and numerical analysis of a new type of solar tower efficiently generating a thermal updraft. *Energies* 2016;**9**:1077. https://doi.org/10.3390/en9121077.
27. Singh AP, Kumar A, Singh OP. A novel concept of integrating bell-mouth inlet in converging-diverging solar chimney power plant. *Renew Energy* 2021;**169**:318–34. https://doi.org/10.1016/j.renene.2020.12.120.
28. Araya HG, Teferi ST. Performance comparison of cylindrical and diverging solar chimney power plants. *Results Eng* 2025;**26**:105485. https://doi.org/10.1016/j.rineng.2025.105485.
29. Adibimanesh B, Ayani MB, Khozeymeh-Nezhad H. *et al.* Applying response surface method to optimize the performance of a divergent-chimney solar power plant. *Sustain Energy Technol Assess* 2021;**48**:101593. https://doi.org/10.1016/j.seta.2021.101593.
30. Ren XH, Meng JJ, Hou BX. *et al.* Configuration optimization and performance analysis of a stepped solar chimney for multiple storey buildings. *Sol Energy* 2026;**303**:114171. https://doi.org/10.1016/j.solener.2025.114171.
31. Torabi MR, Hosseini M, Akbari OA. *et al.* Investigation the performance of solar chimney power plant for improving the efficiency and increasing the outlet power of turbines using computational fluid dynamics. *Energy Rep* 2021;**7**:4555–65. https://doi.org/10.1016/j.egyr.2021.07.044.
32. Hu S, Leung DY, Chan JC. Impact of the geometry of divergent chimneys on the power output of a solar chimney power plant. *Energy* 2017;**120**:1–11. https://doi.org/10.1016/j.energy.2016.12.098.
33. Hassan A, Ali M, Waqas A. Numerical investigation on performance of solar chimney power plant by varying collector slope and chimney diverging angle. *Energy* 2018;**142**:411–25. https://doi.org/10.1016/j.energy.2017.10.047.
34. Ahirwar MJ, Sharma P. Analyzing the effect of solar chimney power plant by varying chimney height, collector slope and chimney diverging angle. *Int J Innov Res Technol* 2019;**6**:213–9.
35. Mandal DK, Biswas N, Manna NK. *et al.* Impact of chimney divergence and sloped absorber on energy efficacy of a solar chimney power plant (SCPP). *Ain Shams Eng J* 2024;**15**:102390. https://doi.org/10.1016/j.asej.2023.102390.
36. Xu Y, Zhou X. Performance of divergent-chimney solar power plants. *Sol Energy* 2018;**170**:379–87. https://doi.org/10.1016/j.solener.2018.05.068.
37. Singh AP, Singh J, Kumar A. *et al.* Vertical limit reduction of chimney in solar power plant. *Renew Energy* 2023;**217**:119118. https://doi.org/10.1016/j.renene.2023.119118.

38. Cuce PM, Sen H, Cuce E. Performance analysis of solar chimney power plant with waste heat integration on the ground. *Int J Ambient Energy* 2025;**46**:2446529. https://doi.org/10.1080/01430750.2024.2446529.
39. Cuce PM, Saxena A, Cuce E. *et al.* Thermal and energy analysis of a novel solar updraft tower design with divergent chimney and convergent collector concept: CFD analysis with experimental validation. *Int J Low-Carbon Technol* 2024;**19**:714–22. https://doi.org/10.1093/ijlct/ctad152.
40. Xu G, Ming T, Pan Y. *et al.* Numerical analysis on the performance of solar chimney power plant system. *Energ Conver Manage* 2011;**52**:876–83. https://doi.org/10.1016/j.enconman.2010.08.014.
41. Asnaghi A, Ladjevardi SM. Solar chimney power plant performance in Iran. *Renew Sustain Energy Rev* 2012;**16**:3383–90. https://doi.org/10.1016/j.rser.2012.02.017.
42. Ganguli AA, Deshpande SS, Pandit AB. CFD simulations for performance enhancement of a solar chimney power plant (SCPP) and techno-economic feasibility for a 5 MW SCPP in an Indian context. *Energies* 2011;**14**:3342. https://doi.org/10.3390/en14113342.
43. Haaf W, Friedrich K, Mayr G. *et al.* Solar chimneys part I: principle and construction of the pilot plant in Manzanares. *Int J Sol Energy* 1983;**2**:3–20. https://doi.org/10.1080/01425918308909911.
44. Mirzamohammad A, Eftekhari Yazdi M, Lavasani AM. Improvement of combined solar chimney power plant with gas power plant. *Sci Rep* 2023;**13**:11220. https://doi.org/10.1038/s41598-023-38464-4.
45. Cuce E, Sen H, Cuce PM. Collector factor in a solar chimney power plant: CFD analysis for the pilot plant in Manzanares. *Energetika* 2022;**68**:33–42. https://doi.org/10.6001/energetika.v68i1.4856.
46. Cuce PM, Cuce E, Alshahrani S. *et al.* Performance evaluation of solar chimney power plants with Bayburt stone and basalt on the ground as natural energy storage material. *Sustainability* 2022;**14**:10960. https://doi.org/10.3390/su141710960.
47. Schlaich J, Bergermann R, Schiel W. *et al.* Sustainable electricity generation with solar updraft towers. *Struct Eng Int* 2024;**14**:225–9. https://doi.org/10.2749/101686604777963883.
48. Kaplan M. Optimization of narrowed chimney section height for improving flow and performance features of a solar chimney power plant: a CFD approach. *Int J Energy Res* 2025;**2025**:1959734. https://doi.org/10.1155/er/1959734.
49. Pastohr H, Kornadt O, Gürlebeck K. Numerical and analytical calculations of the temperature and flow field in the upwind power plant. *Int J Energy Res* 2004;**28**:495–510. https://doi.org/10.1002/er.978.
50. Pasumarthi N, Sherif SA. Experimental and theoretical performance of a demonstration solar chimney model—part I: mathematical model development. *Int J Energy Res* 1998;**22**:277–88. https://doi.org/10.1002/(SICI)1099-114X(19980310)22:3<277::AID-ER380>3.0.CO;2-R.
51. Ming T, Liu W, Pan Y. *et al.* Numerical analysis of flow and heat transfer characteristics in solar chimney power plants with energy storage layer. *Energ Conver Manage* 2008;**49**:2872–9. https://doi.org/10.1016/j.enconman.2008.03.004.
52. Mandal DK, Biswas N, Manna NK. *et al.* An application of artificial neural network (ANN) for comparative performance assessment of solar chimney (SC) plant for green energy production. *Sci Rep* 2024;**14**:979. https://doi.org/10.1038/s41598-023-46505-1.
53. Cottam PJ, Duffour P, Lindstrand P. *et al.* Solar chimney power plants—dimension matching for optimum performance. *Energ Conver Manage* 2019;**194**:112–23. https://doi.org/10.1016/j.enconman.2019.04.074.
54. Gaci F, Azizi MW, Akni A. *et al.* Assessment of solar chimney power plant performance under various parameters. *ITEGAM-JETIA* 2025;**11**:29–47. https://doi.org/10.5935/jetia.v11i55.1854.

International Journal of Low-Carbon Technologies, 2026, 21, 1–14, ctag026
https://doi.org/10.1093/ijlct/ctag026
Original Article